

The ESO UVES Advanced Data Products quasar sample - V. Identifying the galaxy counterpart to the sub-damped Lyα system towards Q 2239-2949

Tayyaba Zafar, Palle Møller, Céline Péroux, Samuel Quiret, Johan P. U. Fynbo, Cédric Ledoux, Jean-Michel Deharveng

▶ **To cite this version:**

Tayyaba Zafar, Palle Møller, Céline Péroux, Samuel Quiret, Johan P. U. Fynbo, et al.. The ESO UVES Advanced Data Products quasar sample - V. Identifying the galaxy counterpart to the sub-damped Lyα system towards Q 2239-2949. Monthly Notices of the Royal Astronomical Society, 2017, 465, pp.1613-1620. 10.1093/mnras/stw2907 . insu-03666209

HAL Id: insu-03666209
https://insu.hal.science/insu-03666209

Submitted on 12 May 2022

HAL is a multi-disciplinary open access archive for the deposit and dissemination of scientific research documents, whether they are published or not. The documents may come from teaching and research institutions in France or abroad, or from public or private research centers.

L'archive ouverte pluridisciplinaire **HAL**, est destinée au dépôt et à la diffusion de documents scientifiques de niveau recherche, publiés ou non, émanant des établissements d'enseignement et de recherche français ou étrangers, des laboratoires publics ou privés.

Monthly Notices
of the
ROYAL ASTRONOMICAL SOCIETY

MNRAS **465,** 1613–1620 (2017)
Advance Access publication 2016 November 14

doi:10.1093/mnras/stw2907

The ESO UVES Advanced Data Products quasar sample – V. Identifying the galaxy counterpart to the sub-damped Lyα system towards Q 2239-2949

Tayyaba Zafar,[1,2★] Palle Møller,[2★] Céline Péroux,[3★] Samuel Quiret,[3] Johan P. U. Fynbo,[4] Cédric Ledoux[5] and Jean-Michel Deharveng[3]

[1]*Australian Astronomical Observatory, PO Box 915, North Ryde, NSW 1670, Australia*
[2]*European Southern Observatory, Karl-Schwarzschild-Strasse 2, D-85748 Garching, Germany*
[3]*Aix Marseille Université, CNRS, LAM (Laboratoire d'Astrophysique de Marseille) UMR 7326, F-13388 Marseille, France*
[4]*Dark Cosmology Centre, Niels Bohr Institute, University of Copenhagen, Juliane Maries Vej 30, DK-2100 Copenhagen, Denmark*
[5]*European Southern Observatory, Alonso de Córdova 3107, Vitacura, Casilla 19001, Santiago 19, Chile*

Accepted 2016 November 7. Received 2016 November 7; in original form 2016 March 7

ABSTRACT

Gas flows in and out of galaxies are one of the key unknowns in today's galaxy evolution studies. Because gas flows carry mass, energy, and metals, they are believed to be closely connected to the star formation history of galaxies. Most of these processes take place in the circum-galactic medium (CGM) which remains challenging to observe in emission. A powerful tool to study the CGM gas is offered by combining observations of the gas traced by absorption lines in quasar spectra with detection of the stellar component of the same absorbing-galaxy. To this end, we have targeted the $z_{\rm abs} = 1.825$ sub-damped Lyα absorber (sub-DLA) towards the $z_{\rm em} = 2.102$ quasar 2dF J 223941.8-294955 (hereafter Q 2239-2949) with the ESO VLT/X-Shooter spectrograph. Our aim is to investigate the relation between its properties in emission and in absorption. The derived metallicity of the sub-DLA with $\log N({\rm H\,I}) = 19.84 \pm 0.14$ cm^{-2} is [M/H] > -0.75. Using the Voigt profile optical depth method, we measure $\Delta v_{90}({\rm Fe\,II}) = 64$ km s^{-1}. The sub-DLA galaxy counterpart is located at an impact parameter of $2\farcs4 \pm 0\farcs2$ (20.8 ± 1.7 kpc at $z = 1.825$). We have detected Lyα and marginal [O II] emissions. The mean measured flux of the Lyα line is $F_{{\rm Ly}\,\alpha} \sim 5.7 \times 10^{-18}$ erg s^{-1} cm^{-2} Å^{-1}, corresponding to a dust uncorrected SFR of $\sim$0.13 M$_\odot$ yr^{-1}.

Key words: galaxies: abundances – galaxies: evolution – galaxies: formation – intergalactic medium – galaxies: ISM – quasars: absorption lines.

1 INTRODUCTION

One of the key unknowns in the study of galaxy evolution is how galaxies acquire their gas and how they exchange this gas with their surroundings. Since gas, stars, and metals are intimately connected, gas flows affect the history of star formation and chemical enrichment in galaxies. Therefore study of the circum-galactic medium (CGM, extending over $\sim$300 kpc around galaxies; Shull, Danforth & Tilton 2014) is crucial for understanding both the inflows of gas accreted on to galaxies and the outflows carrying away the energy and metals generated inside galaxies (Kereš et al. 2012; Ceverino et al. 2016). A powerful tool to study the CGM gas is offered by absorption lines in quasar spectra. Indeed, quasar sightlines provide a wealth of information about the CGM of galaxies through the analysis of the intervening absorption line systems. The detection of the damped Lyα systems (DLAs; $\log {\rm N(H\,I)} \geq 20.3$ cm^{-2}) and sub-damped Lyα systems [sub-DLAs; $19.0 \leq \log {\rm N(H\,I)} < 20.3$ cm^{-2}] in absorption against bright background quasars is in principle not limited by the luminosity of the associated galaxies but depends on the cross-section of the neutral hydrogen gas (e.g. Wolfe et al. 1986). It is now established that gas accretion on global scales is required to reconcile the lack of evolution in the neutral gas mass over large cosmological times with the observed star formation rate (SFR) density evolution (e.g. Noterdaeme et al. 2009; Zafar et al. 2013a; Sánchez-Ramírez et al. 2016). The DLAs and sub-DLAs are therefore excellent laboratories to study metals, molecules, dust, and atomic gas, an indirect indicator of star formation (e.g. Krumholz 2012; Zafar et al. 2013a).

However, the background quasar probes only a single sightline through the galaxy, and it is difficult to study gas flows in the underlying galaxy as a whole from the gas along a single sightline. To establish the connection of the CGM gas probed by the

★ E-mail: tzafar@aao.gov.au (TZ); pmoller@eso.org (PM); celine.peroux@oamp.fr (CP)

© 2016 The Authors
Published by Oxford University Press on behalf of the Royal Astronomical Society

Downloaded from https://academic.oup.com/mnras/article/465/2/1613/2525968 by guest on 12 May 2022

Table 1. Log of spectroscopic observations of Q 2239-2949 from UVES archival and X-Shooter PI time.

Date	T_{exp} (sec)	Instrument	Settings	Slit width (arcsec)	PA (deg)	Resolving power for each arm	Prog. ID	Seeing (arcsec)	Airmass
17 Jun, 2002	1512 × 2	UVES	BLUE437, RED860	1.1		39090, 42310	69.A-0586(A)	1.0	1.1
12 Aug, 2002	3065 × 3	UVES	BLUE346, RED580	1.1		39090, 37820	69.A-0586(A)	0.9	1.0
27 May, 2006	3000	UVES	BLUE346, RED580	1.0		40970, 42310	077.A-0714(A)	1.2	1.8
28 Jun, 2006	3000	UVES	BLUE346, RED580	1.0		40970, 42310	077.A-0714(A)	0.5	1.0
27 Jul, 2006	3000	UVES	BLUE437, RED760	1.0		40970, 42310	077.A-0714(A)	1.5	1.0
15 Jul, 2013	3028[a]	X-Shooter	UVB, VIS, NIR	1.3, 1.2, 1.2	− 14.2	4000, 6700, 3890	091.A-0246(A)	0.7	1.0
31 Jul, 2013	3028	X-Shooter	UVB, VIS, NIR	1.3, 1.2, 1.2	− 72.1	4000, 6700, 3890	091.A-0246(A)	1.0	1.0
	3028	X-Shooter	UVB, VIS, NIR	1.3, 1.2, 1.2	29.2	4000, 6700, 3890	091.A-0246(A)	1.0	1.0
03 Aug, 2013	3028	X-Shooter	UVB, VIS, NIR	1.3, 1.2, 1.2	− 76.3	4000, 6700, 3890	091.A-0246(A)	0.9	1.0
	3028	X-Shooter	UVB, VIS, NIR	1.3, 1.2, 1.2	− 5.2	4000, 6700, 3890	091.A-0246(A)	0.9	1.0
31 Aug, 2013	3028	X-Shooter	UVB, VIS, NIR	1.3, 1.2, 1.2	− 85.5	4000, 6700, 3890	091.A-0246(A)	0.8	1.0

[a]The exposure time for all X-Shooter data is 3000 (UVB), 3028 (VIS), and 960 × 3 (NIR) s. PA convention is East-of-North. The UVES data were obtained with the slit rotating on the sky to follow parallactic angle, so the PA was changing during the exposure.

quasar sightline to the underlying galaxy, it is essential to complement the absorption spectroscopy with studies of the absorbing galaxy in emission, and determine the kinematics and metallicity of the emission-line gas. To reach this goal the first step is to identify DLA host-galaxies in emission in large enough numbers to be able to perform statistical studies (e.g. Péroux et al. 2011; Krogager et al. 2012; Peroux et al. 2017). Until recently, deep, high spatial resolution images were obtained to identify potential DLA galaxies nearby the quasar line of sight (Warren et al. 2001), followed by spectroscopic observations to verify that the galaxies lie at the same redshifts as the DLAs (Weatherley et al. 2005). Today, improved selection strategies using long-slit triangulations (e.g. Fynbo et al. 2011; Noterdaeme et al. 2012; Fynbo et al. 2013; Krogager et al. 2013) or integral field units (e.g. Bouché et al. 2007; Péroux et al. 2012, 2013) have led to several new spectroscopic detections of DLA galaxies in emission.

In parallel, the discovery that high-z DLA galaxies obey luminosity–metallicity and velocity–metallicity relations with similar slopes as in the local Universe, Møller, Fynbo & Fall (2004), Ledoux et al. (2006), and Neeleman et al. (2013) allow one to relate flux limited galaxy samples and DLA selected samples (Møller et al. 2013; Christensen et al. 2014). Establishing this connection reinforces the possibility of quasar absorbers to trace the evolution of faint galaxies even back to redshifts where they are too faint to be seen in emission (Fynbo et al. 2008). It is therefore of high importance to extend the sample of DLA galaxies seen in emission, and to extend the parameter space of detections [e.g. to lower H I column densities (sub-DLAs) and to lower metallicities] to better probe the faint-end of the galaxy luminosity function.

Here, we report the detection of a new absorbing-galaxy in the field of Q 2239-2949. The quasar ($z_{em} = 2.102$, $B = 19.31$ mag) was first discovered in the 2-degree Field (2dF) survey at the Anglo Australian Telescope (Croom et al. 2001). Using ESO/UV and Visual Echelle Spectrograph (UVES) archival data, Zafar, Popping & Péroux (2013b) report the detection of Lyα flux in emission in the trough of the sub-DLA at $z = 1.825$ in the sightline towards Q 2239-2949. In this paper, we present new X-Shooter observations of the absorbing-galaxy detected in emission which allows one to characterize the properties of its stellar components as well as a complete analysis of archival UVES data to extract fundamental parameters of the neutral gas seen in absorption.

We adopt the standard ΛCDM cosmology with the cosmological parameters $\Omega_\Lambda = 0.73$, $\Omega_m = 0.27$, and $H_0 = 70\,\mathrm{km\,s^{-1}\,Mpc^{-1}}$.

2 OBSERVATIONS AND DATA REDUCTION

2.1 UVES spectroscopy

The quasar Q 2239-2949 was first observed with UVES (Dekker et al. 2000) with three different settings as part of the tomography of the intergalactic medium programmes (69.A-0586(A) PI: Cristiani, 077.A-0714(A) PI: D'Odorico). The EUADP (ESO UVES Advanced Data Products) archival data (Zafar et al. 2013a,b) did not include all the data taken on that object, therefore, we retrieved the additionally available raw data and reduced it using the UVES pipeline 5.4.0 (Ballester et al. 2000). The complete log of observations is provided in Table 1.

The raw frames are corrected for bias level, flat-field, and rectified in wavelength space using a wavelength solution obtained from calibration frames. The orders are then merged and 1D spectra are extracted from the merged 2D spectra. The resulting spectrum ranges from 3024 to 10 433 Å. The spectra from different settings are corrected to the vacuum heliocentric reference system and merged into a single spectrum following the method described by Zafar et al. (2013b). The merged quasar continuum is then normalized by fitting a spline function passing through spectral chunks of 200 Å apparently devoid of absorption lines.

2.2 X-Shooter spectroscopy

During our inspection of the initial UVES data, we noted that Lyα emission flux from the absorbing galaxy is detected in the trough of the absorption in individual UVES spectra [see fig. 20 of Zafar et al. (2013b)]. In order to precisely measure the position on sky, impact parameter as well as the emission properties of the galaxy traced by its Lyα emission, we then re-observed Q 2239-2949 with VLT/X-Shooter (Vernet et al. 2011) using six different 'Observation Blocks' under program ID 091.A-0246(A) (PI: Zafar; observing log provided in Table 1). The exposure times were 1 h each. The observations were made in 'STARE mode' because the position of the sub-DLA galaxy on sky was unknown. Indeed, the 'STARE mode' helps to avoid the quasar counter-image to fall on top of the galaxy, but the absence of telescope nodding then limits the quality of the NIR arm. The slit widths were 1.3 arcsec, 1.2 arcsec, and 1.2 arcsec in the UVB, VIS, and NIR arms, respectively. The expected resolving power with the above set-up, and for seeing matching the slits, is 4000, 6700 and 3890 in the UVB, VIS and NIR arms, respectively. Those resolutions are computed from the slit

Downloaded from https://academic.oup.com/mnras/article/465/2/1613/2525968 by guest on 12 May 2022

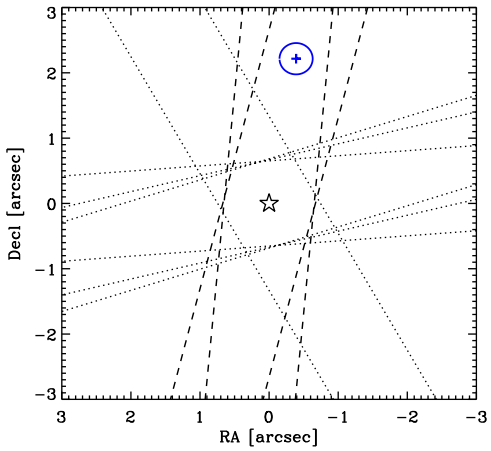


Figure 1. Slit positions used for the X-Shooter observations of Q 2239-2949 (marked by a star). The dashed lines show the slit positions PA = −14° and −5°, where we detect emission-line flux from the sub-DLA galaxy. The probable position of the galaxy is marked by a cross and a blue circle at an impact parameter of 2″.4. At other slit positions (dotted lines) no emission-line flux is detected.

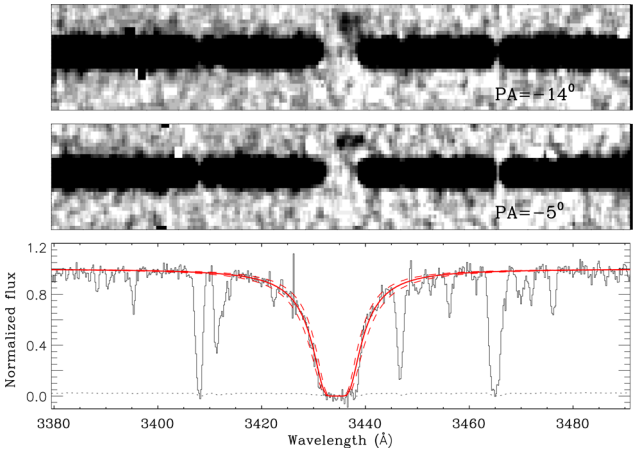


Figure 2. The sub-DLA emission and absorption. The upper two panels show the 2D spectra from the PAs −14° and −5°. The Lyα emission from the sub-DLA-galaxy counterpart is seen close to the red wing of its absorption line, offset by 2.4 arcsec upwards from the quasar spectrum. In the lower panel we show the combined, extracted 1D spectrum of the QSO and its corresponding noise spectrum (dotted line). The red solid and dashed lines show the best-fitting H I column density profile ($z = 1.825$, log N(H I) = 19.78 ± 0.11 cm^{-2}) and its 1σ uncertainty, respectively.

widths, assuming that the slit is matched to the seeing. However, since we were searching for line emission from a source at an unknown position we used slits wider than the seeing, and the actual point-source resolutions, based on the median seeing of 0.9 arcsec, are 5330, 8930, and 5190. We requested the observations to be performed in service mode but erroneously set the rotator angle to parallactic at the start of each observations. Fortunately, the PAs cover the regions around the QSO fairly well (see Fig. 1) and we detect the source in the spectra with PA of −14° and −5° (East-of-North).

The X-Shooter spectra are reduced with the X-Shooter pipeline 2.4.0 (Modigliani et al. 2010). The standard procedures within STARE mode for master bias, master dark, flat-fielding, wavelength calibration, and the 2D maps for rectification of the spectra are performed. The flux standard stars EG 274 (on 2013 July 15 and August 31) and Feige 110 (on 2013 July 31 and August 03) are observed and used to flux calibrate the science spectra of the corresponding nights. The resulting flux-calibration is not absolute, but rather removes the instrumental effects from the quasar continuum.

The spectra were corrected for galactic extinction (E_{B-V} = 0.019) using the extinction maps of Schlegel, Finkbeiner & Davis (1998). In Fig. 2, we present the section around the DLA of the extracted 2D spectra at PAs = −14° and −5° (top two panels) and the final combined 1D QSO spectrum (bottom panel). We clearly detect the Lyα emission in both spectra (the dark blobs above the 2D QSO spectrum). The Lyα emission is well separated from the QSO spectrum and is therefore not present into the 1D QSO spectrum.

3 RESULTS

3.1 Gas absorption properties and metallicity

Zafar et al. (2013b) reported an H I column density of the sub-DLA of log N(H I) =19.84 ± 0.14 cm^{-2}. The X-Shooter data are also used to derive the H I column density and the estimated column density is log N(H I) =19.78 ± 0.11 cm^{-2} (Fig. 2), consistent with the UVES results within 1σ.

The high-resolution UVES spectrum allows us to perform absorption line profile fitting and determine the column densities from lines that are not heavily saturated. The column densities have been derived using the Voigt profile fitting, χ^2 minimization routine FITLYMAN within the MIDAS environment (Fontana & Ballester 1995). Laboratory wavelengths and oscillator strengths are taken from Morton (2003). The global fit returns the best-fitting parameters for the central wavelength, column density, and Doppler turbulent broadening (b), as well as 1σ errors on each quantity.

Absorption lines detected from Si II, Fe II, and Al III display a multicomponent structure covering ∼80 km s^{-1} around $z_{\rm abs} = 1.825$. A first velocity profile estimation is manually derived for Fe II 2260, 1608, 2374 and 2344 Å. Seven components are used to model the observed absorption lines. This approach forces FITLYMAN to converge towards the optimal solution. Si II 1808 and 1304 Å lines are added, maintaining the redshifts and Doppler parameters previously derived, thereby providing the initial solution for the Si II column density. Thus, the software is run again fully using these parameters as first guest solutions. We finally added Al III 1862 and perform again the previous operation. The resulting Doppler parameter for the third component (b= 1.2 km s^{-1}) is so small that it might be unphysical. For this reason, a value of $b = 3$ km s^{-1} is enforced and the fit is performed again. The simultaneous multiple Voigt profile fitting is shown in Fig. 3. For saturated and non-detected lines, we report 3σ column density lower and upper limits, respectively (see Table 2). The overall measured, i.e. before considering a possible ionization correction, sub-DLA metallicity is found to be [Si/H] = −0.67 ± 0.15.

As a consistency check we compare our absorption line results with the X-Shooter data. We measure the rest equivalent widths of unsaturated lines and find $W_{\rm r}^{\lambda 1808} = 0.02 \pm 0.03$ Å, $W_{\rm r}^{\lambda 2374} = 0.16 \pm 0.04$ Å, and $W_{\rm r}^{\lambda 1862} = 0.08 \pm 0.03$ Å, for Si II, Fe II, and Al III, respectively. Using those equivalent widths, and assuming the lines to be on the linear part of the curve-of-growth, we determine the column densities log N(Si II) =14.48 ± 0.19 cm^{-2}, log N(Fe II) =14.01 ± 0.10 cm^{-2}, and log N(Al III) =12.97 ± 0.14 cm^{-2} in full agreement with the UVES data.

The error on the [Si/H] metallicity given above includes only the observational errors. It is well known that for sub-DLAs there may

Downloaded from https://academic.oup.com/mnras/article/465/2/1613/2525968 by guest on 12 May 2022

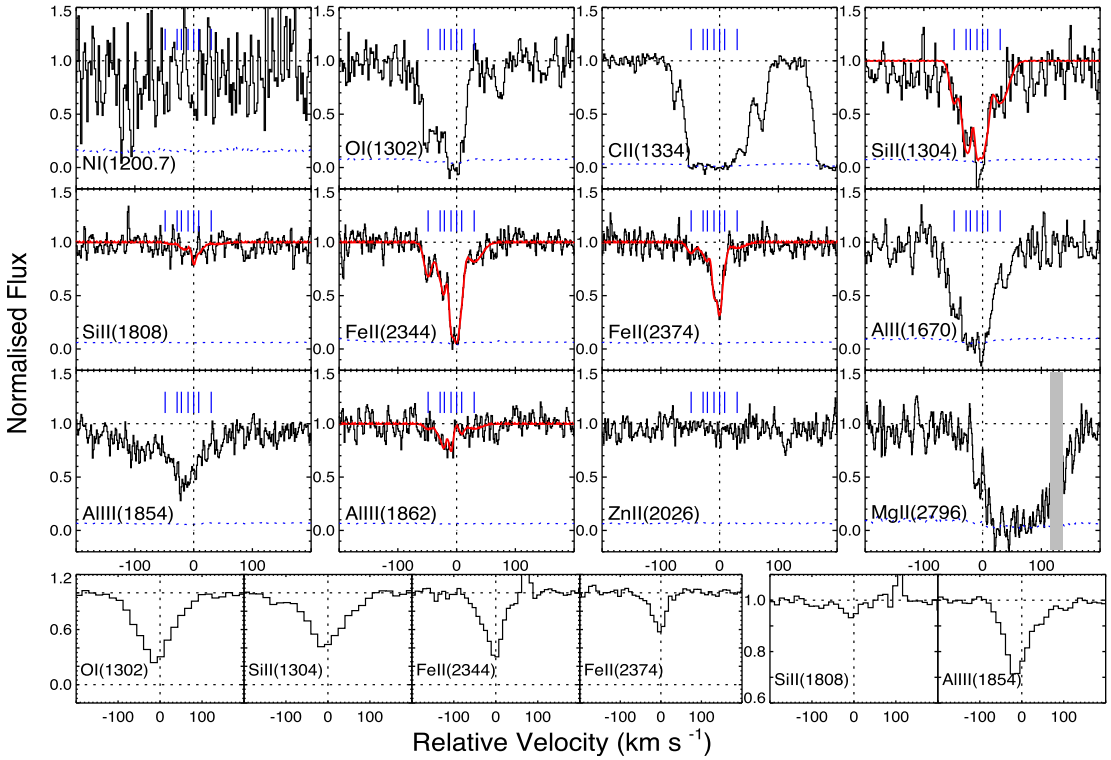


Figure 3. Voigt-profile fits (red overlay) of metal lines for the sub-DLA at $z_{\rm abs} = 1.82516$ (zero velocity) in Q 2239-2949. Normalized quasar spectrum and error spectrum are shown in black and blue dotted lines, respectively. The blue tick marks indicate the locations of the velocity components. The grey shaded area marks contamination from a telluric absorption line. The top three rows present the UVES data and fits, the bottom row presents some of the same lines from the X-Shooter spectrum as useful comparison. For instance, it is seen that the depression of Al III (1854 Å) at around $-100\,{\rm km\,s^{-1}}$ in the UVES spectrum is not seen in the X-Shooter spectrum so it is probably not real. All the other lines are fully consistent in both spectra.

Table 2. Metallicity with respect to solar of the sub-DLA.

X	log N_X (cm^{-2})	[X/H]	[X/H]$^a_{\rm tot}$
H I	19.84 ± 0.14	–	–
N I	<14.71	<−0.96	–
Zn II	<12.30	<−0.10	–
Si II	14.68 ± 0.06	-0.67 ± 0.15	–
O I	>16.08	>−0.45	–
C II	>15.97	>−0.30	–
Fe II	14.11 ± 0.04	-1.23 ± 0.15	–
Al III	12.87 ± 0.07	–	–
Al II	>13.61	>−0.68	>−0.61
Cr II	<12.79	<−0.69	–
Mg II	>14.86	>−0.58	>−0.58
Mg I	<12.96	–	–

[a]Total abundances from the sum of all listed ionization states.

be a large range of possible ionization levels, which would cause additional uncertainty on the metallicity unless the ionization parameter can be constrained. While the gas in the sub-DLAs is found to range from predominantly ionized to predominantly neutral (Meiring et al. 2007, 2009; Lehner et al. 2014; Fumagalli, O'Meara & Prochaska 2016), the relative ionization correction varies from element to element (e.g. <0.2 dex for Fe II). Our [Si/H] metallicity could therefore be affected by ionization effects, by dust depletion, or the combination of both. The measured [Si/Fe] ratio indeed indicates that at least one of these two effects is at play, if not both of them.

Unfortunately we have, in the present case, only a limit on the Al III/Al II ratio, which may not be a reliable indicator of the ionization parameter because the recombination coefficient of Al II is likely overestimated (Nussbaumer & Storey 1986). Our best constraint is therefore that of [O/H]>−0.45 which is independent of the ionization effects for this H I column density, and we will simply rely on this throughout the paper. Because α-elements may be enhanced by up to a factor of 2, the lower limit on the actual metallicity is −0.75 (3 σ).

3.2 Emission lines

The detection of Lyα in emission above the position of the QSO is clear from Fig. 2. The impact parameter is large enough that the faint Lyα emission does not show up in the extracted QSO spectrum, but there is a small overlap which would leave a residual of the bright QSO in the DLA galaxy spectrum if not corrected for. Therefore, in order to extract the 1D spectrum of the Lyα emission line we must first spectral point spread function (SPSF) subtract the QSO 2D spectrum in the overlapping region (Møller 2000). Because the seeing is different in the two exposures, we perform the SPSF subtraction on the two spectra individually, then add them. The resulting 2D frame is seen in the lower panel of Fig. 4 (boxcar smoothed for presentation purposes).

From the non-smoothed, summed, and SPSF subtracted 2D spectrum we then extract the 1D spectrum shown in the top panel of

Downloaded from https://academic.oup.com/mnras/article/465/2/1613/2525968 by guest on 12 May 2022

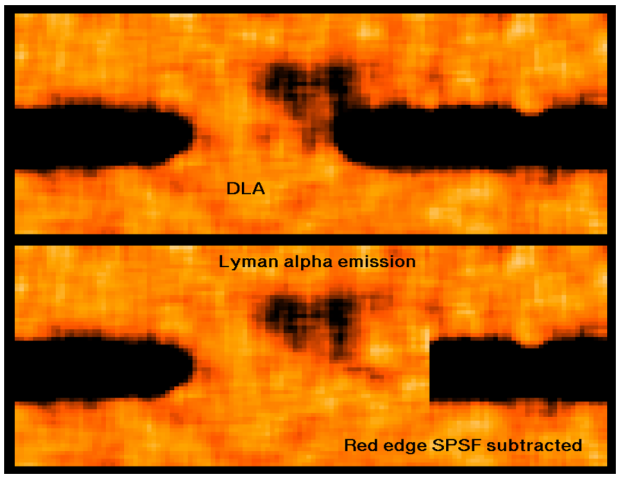


Figure 4. Stack of Lyα emission from the sub-DLA observed at PA $= -14^\circ$ and -5°. The top panel shows the direct stack, while in the lower panel each spectrum was SPSF subtracted at the red side of the DLA line prior to the summing. There is evidence that the Lyα emission has two peaks.

Fig. 6. It is seen that all Lyα emission is to the right-hand (high redshift) side of the absorber, i.e. that the profile matches the typical high-redshift profile with a blue cut-off and a red tail (e.g. Francis et al. 1996; Castro-Tirado et al. 2010; Hu et al. 2010; Noterdaeme et al. 2014). However, in this case it is also seen that the profile appears to be double peaked. In the figure, we have therefore fitted the profile with a double Gaussian, and find that it is fitted well by two Gaussian profiles (shown red in overlay) centred on 3435.9 and 3438.6 Å with the measured FWHM of 1.7 Å and 2.1 Å, respectively. After correction for resolution the intrinsic FWHM is found to be 1.5 and 1.9 Å, corresponding to 130 and 165 km s^{-1}. The separation between the two peaks corresponds to 230 ± 40 km s^{-1}. The two peaks are seen to be clearly separated also in the stacked 2D spectrum.

The measured flux of the Lyα emission line in the two spectra is $F_{\mathrm{Ly}\alpha} = 5.1 \pm 0.8 \times 10^{-18}$ erg s^{-1} cm^{-2} Å^{-1} and $6.2 \pm 0.8 \times 10^{-18}$ erg s^{-1} cm^{-2} Å^{-1} for PA $= -14^\circ$ and -5°, respectively. The two measurements are fully consistent with each other, but they obviously only include the flux passing through the slit in each case. Different slit PA and different seeing causes the slit loss to be different for the two observations, so part of the difference may reflect the two setups. Together the two measurements provide a 10σ detection of the Lyα emission. We convert the Lyα luminosity density to SFR using the relation from Kennicutt (1998): SFR ($\mathrm{M}_\odot$ yr^{-1}) $= 7.9 \times$ L(Hα) (erg s^{-1}) and case B recombination theory for flux ratio conversion: Lyα/Hα $= 8.7$. We find that the measured fluxes correspond to a dust uncorrected $\mathrm{SFR}_{\mathrm{Ly}\alpha}$ of 0.13 ± 0.02 $\mathrm{M}_\odot$ yr^{-1}. The true value is likely to be somewhat higher due to unknown slit loss corrections. We estimate (based on slit width and seeing) that this correction is less than a factor of 2, i.e. $\mathrm{SFR}_{\mathrm{Ly}\alpha}$ is in the range 0.11–0.26 $\mathrm{M}_\odot$ yr^{-1}.

We searched the spectrum for other emission lines and found marginal evidence for [O II] line emission in the NIR spectrum at the same impact parameter as for Lyα (2.4 arcsec) and is roughly centred on the sub-DLA absorption lines, contrary to the Lyα emission. Also as for Lyα the line is found to be stronger and better detected at PA $= -5^\circ$ than at PA $= -14^\circ$. In Fig. 5, we show the sum of the two spectra. The [O II] doublet is partly hidden behind the strong residuals left from the subtraction of an airglow line. For presentation purposes, in Fig. 5 we have smoothed the spectrum

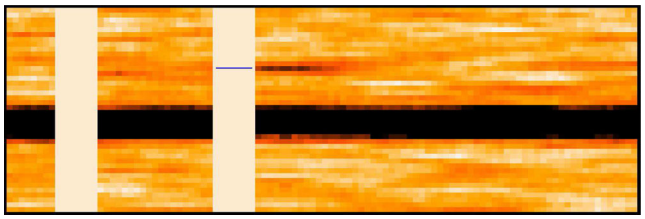


Figure 5. Section of the 2D spectrum (sum of PA $= -5^\circ$ and -14° spectra) around the expected wavelength of the [O II] doublet. The spectrum has been smoothed along the dispersion direction to enhance the visibility of the [O II] line which is seen as a dark feature above the quasar spectrum. The residuals from the subtraction of two strong air glow lines have been masked out (vertical bands) and the horizontal blue line in the rightmost of those marks the 2.4 arcsec impact parameter of the Lyα emission for comparison.

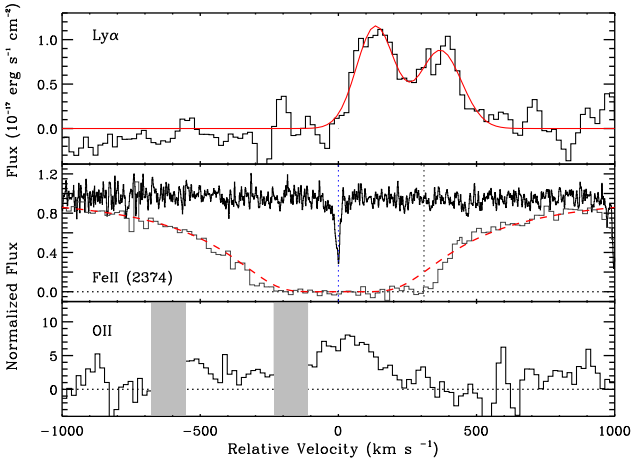


Figure 6. Velocities of absorption and emission components relative to $z = 1.82516$. In the middle panel the H I absorption profile is overlaid on the un-saturated profile of a Fe II absorption line. Note the additional absorption component at $v \approx 300$ km s^{-1} in the H I absorption profile (black vertical dotted line). In the top panel, we show the double-peaked profile of the Lyα emission from the galaxy (black) with a fit of two Gaussian profiles (red). The bottom panel shows the extracted spectrum at the expected position of the [O II] doublet (grey shaded areas mark positions of masked air glow lines). A marginal detection is achieved.

along the dispersion direction and masked out the residuals of the two strong airglow lines. The 1D spectrum of the [O II] line is shown in the lower panel of Fig. 6.

3.3 Gas kinematics

We have detected Lyα and [O II] emission from the host galaxy of the sub-DLA system, providing us with an opportunity to study the gas kinematics of the galaxy probed at two different locations. In Fig. 6, we summarize the kinematic information of all the gas components, plotting them in velocity relative to a fiducial redshift chosen to be $z = 1.82516$. It is seen that H I and the low-ion metal lines are lined up at the same central redshift in the absorption sightline, but also that the [O II] emitting gas some 20.8 kpc away has the same redshift. We measure a central wavelength of the [O II] doublet of 10 533.9 Å $\pm$ 1.5 corresponding to a relative velocity of $v = 10 \pm 42$ km s^{-1}. In effect this means that the neutral sub-DLA gas is at rest (radially) with respect to the galaxy, whereas the Mg II absorbing gas extends out to $+170$ km s^{-1} in radial velocity (Fig. 3). I.e. where the narrow line sub-DLA phase appears to be

Downloaded from https://academic.oup.com/mnras/article/465/2/1613/2525968 by guest on 12 May 2022

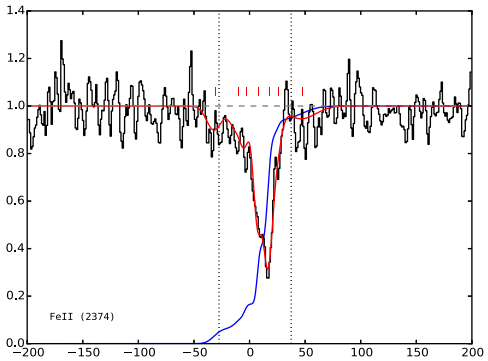


Figure 7. VPOD method (Quiret et al. 2016) relying on the Voigt profile fit of multiple transitions of the same ion. The fit is shown here in red, the integrated optical depth in blue and the observed spectrum for the Fe II (2374 Å) transition is shown in black for illustration purpose. This method is therefore independent of blending, saturation, and noise in the spectrum.

at rest inside the extended halo, at least part of the Mg II absorbing gas belongs to a more turbulent component.

In contrast to the relative velocity agreement for [O II], the Lyα emission has a complex 'double hump' structure with both peaks offset towards higher redshifts. Double-peaked Lyα emission has been reported in relation to DLAs in the past (e.g. Fynbo et al. 2010; Zafar et al. 2011; Noterdaeme et al. 2012), but in the form of two peaks straddling a central absorption feature at the systemic redshift. Verhamme et al. (2008) analysed Lyα emission lines in a sample of 11 high-redshift galaxies from the FORS deep field. To obtain high enough signal-to-noise ratio (S/N) for their analysis they were restricted to include only the intrinsically brightest galaxies, and only those with the largest Lyα equivalent widths. All 11 galaxies feature the sharp blue cut-off of the Lyα emission, as well as the tail towards the red. Interestingly two of the galaxies also show a secondary hump well to the red of the first peak and at about $+300\,\mathrm{km\,s^{-1}}$ with respect to the galaxy redshift. In that work this was taken as evidence for gas outflow, but the same line structure could simply be the result of superposition of two single lines, i.e. two individual Lyα emitting clouds, at slightly different velocities.

In the case of Q2239-2949 the secondary peak is offset by $+400\,\mathrm{km\,s^{-1}}$, and we note that on the red side of the sub-DLA trough an additional absorption feature is seen at $\approx 300\,\mathrm{km\,s^{-1}}$. This is most likely a Lyα absorption line and could in that case be arising in a separate absorbing cloud in the CGM of the galaxy. In this case it might be related to the second peak of the Lyα emission complex. We do not detect any metal lines associated with the secondary absorption component.

In order to derive the internal kinematics of the absorbing gas, we calculate the absorption line velocity width, Δv_{90} (Prochaska & Wolfe 1997; Ledoux et al. 2006). For this, it is standard practice to carefully select a line (if possible more than one) which is unsaturated, unblended, and of sufficiently high S/N [for details see e.g. Ledoux et al. (2006)]. An alternative method is to measure Δv_{90} on the combined information from several lines of the same transition via the Voigt profile optical depth (VPOD; Quiret et al. 2016). This method also overcomes possible effects from the differential instrumental resolutions, line spread functions and SNRs as well as blending/saturation in the absorption profiles.

In the UVES spectrum of Q 2239-2949 there is no perfect line to measure, and we have therefore adopted the VPOD method and used a combined Voigt profile fit to two lines of Fe II. Fig. 7 shows the resulting integrated optical depth for the Fe II (2374 Å) with inferred velocity widths of $\Delta v_{90}(\mathrm{Fe\ II}) = 64\,\mathrm{km\,s^{-1}}$. The X-Shooter data have lower resolution, but higher S/N, and since we know from the model fit that the Fe II (2374 Å) line is unsaturated, we can obtain a direct measurement from this line, and we find $83\,\mathrm{km\,s^{-1}}$. Because of the lower resolution of X-Shooter this value needs to be corrected for resolution, and following the method described in equation (1) of Arabsalmani et al. (2015) we obtain an intrinsic value of $68\,\mathrm{km\,s^{-1}}$. The two methods and the two data sets are therefore in excellent agreement.

3.4 Impact parameter

We detect Lyα emission (see Fig. 4) at the -14° and -5° position angles. We also detect [O II] at lower S/N (see Fig. 5). Unfortunately, the H α, H β, [N II], and [O III] lines all fall on telluric regions, and are therefore unaccessible. The angular separation between the QSO and the sub-DLA galaxy can be converted to the projected galaxy impact parameter, yielding information about the gaseous extent of the galaxy halo. Using both the Lyα and the [O II] lines we measure the impact parameter between the QSO and the sub-DLA galaxy (Figs 4 and 5) to be $b = 2\farcs4 \pm 0\farcs2$, corresponding to 20.8 ± 1.7 kpc at $z = 1.825$.

3.5 Dust properties

Presence of dust within the absorber will have two effects. First it will result in a depletion of certain metals on to the dust grains, secondly it could cause a general reddening of the continuum. The non-detections of many elements and the saturation of other lines make it hard to infer precise dust depletion fractions, instead we are able to set limits on the depletion factor of iron compared to zinc: [Zn/Fe] <1.13. The value indicates higher amount of depletion with respect to the typical values for DLAs (Noterdaeme et al. 2008; De Cia et al. 2016).

Comparing our X-Shooter spectrum of Q 2239-2949 (scaled to the 2dF b-band photometry) to the quasar template spectrum from Vanden Berk et al. (2001) and Glikman, Helfand & White (2006), and using the Small Magellanic Cloud extinction law from Pei (1992), we find no evidence of dust reddening with $E(B-V) < 0.02$. However, we stress the limitations of this approach. First, the X-Shooter flux calibration is not absolute and we performed no correction for slit-loss. Given that quasars are known to be variable objects (Palanque-Delabrouille et al. 2016), the rescaling to the 2dF b-band photometry might not totally overcome these drawbacks. Furthermore, intrinsic colours of quasars are also known to vary from one object to another so that a comparison to a quasar template does not directly untangle reddening of the background quasar from reddening of the intervening absorber (Péroux et al. 2014).

4 SUMMARY AND DISCUSSION

We have presented new X-Shooter data, as well as previously unpublished archival UVES data, of the $z = 1.82516$ intervening sub-DLA absorber towards the quasar Q 2239-2949. We combined those data with a re-analysis of previously published archival UVES data. Our results can be summarized as follows.

(i) We report the detection of the absorbing galaxy in emission. The galaxy is clearly detected in Lyα at high S/N and the emission line is resolved. In addition a tentative detection of [O II] is reported. However, the sky subtraction residuals in the X-shooter

Downloaded from https://academic.oup.com/mnras/article/465/2/1613/2525968 by guest on 12 May 2022

data are significant, and the reality of the [O II] line detection requires independent confirmation.

(ii) *PA and impact parameter.* The detection of the absorbing galaxy was secured using the 'slit triangulation' technique. It was detected at slit position angles PA $= -14^\circ$ and -5°. Using this, together with its position in the slits, we find that the most likely position of the galaxy is at a PA (E of N) of $-10^\circ \pm 15^\circ$, and an impact parameter of $2\farcs4 \pm 0\farcs2$, or 20.8 ± 1.7 kpc.

(iii) *SFR.* We measure a Lyα line flux of $F_{\mathrm{Ly}\alpha} = 5.7 \times 10^{-18}$ erg s^{-1} cm^{-2} Å^{-1}, corresponding to a dust uncorrected SFR of 0.13 M$_\odot$ yr^{-1}. Because of the large impact parameter, the uncertainty in the position angle of the emitter, and the unknown physical size of the line-emitting region, slit losses are likely to be significant (we estimate up to a factor of 2), and the inferred SFR will then be a similar factor higher.

The unknown dust correction could be even more important. It is well known that the dust absorption of Lyα photons can cause an additional underestimate of the SFR. An estimate of this effect can be obtained from the observation of both IR continuum and Lyα-based SFRs, in a sample of narrow band Lyα selected galaxies out to a redshift of $z = 2.3$ (Nilsson & Møller 2009). From their fig. 3 it is seen that the measured correction ranges from a factor of 1 to 2×10^3. It is also seen that the correction strongly correlates with the reddening, and the largest corrections are all corresponding to super massive ULIRGs. In Section 3.5, we report evidence for a relatively high amount of dust depletion in this sub-DLA, but we see no direct evidence for reddening of the QSO continuum. We conclude that in this sightline there is some dust present, but not enough to cause a detectable reddening signature. From Nilsson & Møller (2009) we then conclude that if this sightline is typical for the galaxy, then the SFR dust correction is almost certainly less than a factor of 10. It is possible that other sightlines through the galaxy may contain more dust, additional data are required to answer this question.

(iv) *Kinematics and velocity width.* We measure the Δv_{90} parameter of the absorption system both directly on the data, and on the fitted Voigt profile model. We find that the two methods give consistent results, and we adopt $\Delta v_{90} = 64$ km s^{-1} as the best value. The Lyα emission line displays the typical features of a sharp blue cut-off at the absorption redshift and an extended red tail. In this object the red tail appears to have an additional hump, which is significantly offset ($+230 \pm 40$ km s^{-1}) from the main peak. This second peak may be interpreted in terms of radiation transfer in the case of large-scale outflows, but could also simply be related to the Lyα absorption line seen at a similar redshift.

The tentative detection of an [O II] emission line is at a relative velocity of $+10 \pm 40$ km s^{-1}. From the compilation of relative velocities of [O II] emission in table 6 of Fynbo et al. (2013), we find that values lie in the range 9–200 km s^{-1} with a median of 38 km s^{-1}. This new system is therefore in excellent agreement with previous studies. Since the [O II] redshift is our best estimator for the systemic redshift, we take this to mean that the absorbing sub-DLA phase kinematics is not only internally very narrow, but it also appears to be almost at rest with respect to the galaxy 20.8 kpc away. I.e. the cold CGM at this position does not seem to be wildly turbulent or disturbed.

(v) *Metallicity and impact parameter relations.* We measure a metallicity of [O/H] > -0.75 for the sub-DLA at $z = 1.82516$ with N(H I) $= 19.84 \pm 0.14$ cm^{-2}. A larger impact parameter for lower column density systems has been consistently predicted by numerical simulations for decades (e.g. Katz et al. 1996; Pontzen et al. 2008), and has equally consistently been confirmed by observations (Møller & Warren 1998; Monier, Turnshek & Rao 2009; Péroux et al. 2011; Rao et al. 2011). Similarly, an impact parameter versus metallicity relation was predicted by Møller et al. (2004) and confirmed by Krogager et al. (2012).

Based on observations of several types of high-redshift galaxies, Fynbo et al. (2008) formulated an empirical model to fit DLA galaxies, GRB host galaxies, and Lyman Break Galaxies with a single model. The model has proven useful for predicting and describing the statistical distributions of the DLA galaxy scaling relations, and has been confirmed by the current larger statistical sample compiled by Krogager et al. (2012). Comparing our new sub-DLA galaxy to the relations shown in fig. 3 of that paper, shows that it falls perfectly on both relations. It seems to be a prototypical sub-DLA galaxy.

(vi) *Are sub-DLAs dynamically different from DLAs?* Meiring et al. (2007) and Kulkarni et al. (2010) have shown that the sub-DLAs have higher metallicity than the DLAs when the two systems have the same Δv_{90}. They suggest that this could mean that the sub-DLA galaxies and DLA galaxies are different, and have different masses. The observation could however more simply be understood by stating that, for the same metallicity (i.e. same mass) a sub-DLA has a narrower absorption line profile than a DLA. In the context of the galaxy we report here, we confirm that indeed the absorption would be expected to have $\Delta v_{90} > 207$ km s^{-1} for a DLA [using the optimal fits from Møller et al. (2013) and including the redshift evolution], which is significantly wider than the 64 km s^{-1} we measure. We also find a large impact parameter (20.8 kpc), and further find that the absorber has a very low velocity with respect to the systemic velocity of the galaxy. We take those observations to support the view that the sub-DLAs likely belong to the same galaxies as the DLAs, but that they are caused by gas in the outskirts of the galaxy haloes whereas the DLAs belong to gas closer to the galaxy itself, or even to gas inside the galaxy. Support for this also comes from the observations of GRB sightlines which go through the central parts of galaxies and follow the same relations as intervening DLAs (Arabsalmani et al. 2015).

(vii) *Is this sub-DLA on the main sequence of star formation?* Based on the observed metallicity lower limit, redshift, and impact parameter, we use the prescription in Christensen et al. [2014, their equation (3)] to determine the corresponding stellar mass limit and find $\log(\mathrm{M}_*/\mathrm{M}_\odot) > 9.5 \pm 0.4$. We have here adopted the reported scatter (0.39) as the error, but it should be kept in mind that for the sub-DLAs the scatter of that relation may be larger (Kulkarni et al. 2010). In Section 3.2, we found a dust uncorrected SFR of 0.13 M$_\odot$ yr^{-1}, but at $z = 1.8$ a main sequence galaxy of this mass has a much higher SFR (Whitaker et al. 2014; Kochiashvili et al. 2015). Even applying the maximum correction for dust and slit losses (a factor of 20) it is still about one order of magnitude too low. This indicates that either the true SFR correction is indeed an order of magnitude higher (i.e. there is more dust closer to the centre of the galaxy), or this galaxy has been quenched and is well below the main sequence. An observational determination of both the stellar mass and SFR for this galaxy is possible with current instrumentation, and would settle the issue directly.

ACKNOWLEDGEMENTS

The research leading to these results has received funding from the European Research Council under the European Union's Seventh Framework Program (FP7/2007-2013)/ERC Grant agreement no. EGGS-278202. CP and SQ would like to thank the BINGO! ('history of Baryons: INtergalactic medium/Galaxies cO-evolution')

Downloaded from https://academic.oup.com/mnras/article/465/2/1613/2525968 by guest on 12 May 2022

project by the Agence Nationale de la Recherche (ANR) under the allocation ANR-08-BLAN-0316-01. CP thanks the ESO science visitor program for support. *Facilities*: Based on the observations collected during programmes ESO 069.A-0586, 077.A-0714 and 091.A-0246 at the European Southern Observatory with UVES and X-Shooter on the 8.2 m telescopes operated at the Paranal Observatory, Chile.

REFERENCES

Arabsalmani M., Møller P., Fynbo J. P. U., Christensen L., Freudling W., Savaglio S., Zafar T., 2015, MNRAS, 446, 990
Ballester P., Modigliani A., Boitquin O., Cristiani S., Hanuschik R., Kaufer A., Wolf S., 2000, The Messenger, 101, 31
Bouché N., Lehnert M. D., Aguirre A., Péroux C., Bergeron J., 2007, MNRAS, 378, 525
Castro-Tirado A. J. et al., 2010, A&A, 517, A61
Ceverino D., Sanchez-Almeida J., Muñoz-Tuñon C., Dekel A., Elmegreen B. G., Elmegreen D. M., Primack J., 2016, MNRAS, 457, 2605
Christensen L., Møller P., Fynbo J. P. U., Zafar T., 2014, MNRAS, 445, 225
Croom S. M., Smith R. J., Boyle B. J., Shanks T., Loaring N. S., Miller L., Lewis I. J., 2001, MNRAS, 322, L29
De Cia A., Ledoux C., Mattsson L., Petitjean P., Srianand R., Gavignaud I., Jenkins E. B., 2016, preprint (arXiv:1608.08621)
Dekker H., D'Odorico S., Kaufer A., Delabre B., Kotzlowski H., 2000, in Iye M., Moorwood A. F., eds, Proc. SPIE Conf. Ser. Vol. 4008, Optical and IR Telescope Instrumentation and Detectors. SPIE, Bellingham, p. 534
Fontana A., Ballester P., 1995, The Messenger, 80, 37
Francis P. J. et al., 1996, ApJ, 457, 490
Fumagalli M., O'Meara J. M., Prochaska J. X., 2016, MNRAS, 455, 4100
Fynbo J. P. U., Prochaska J. X., Sommer-Larsen J., Dessauges-Zavadsky M., Møller P., 2008, ApJ, 683, 321
Fynbo J. P. U. et al., 2010, MNRAS, 408, 2128
Fynbo J. P. U. et al., 2011, MNRAS, 413, 2481
Fynbo J. P. U. et al., 2013, MNRAS, 436, 361
Glikman E., Helfand D. J., White R. L., 2006, ApJ, 640, 579
Hu E. M., Cowie L. L., Barger A. J., Capak P., Kakazu Y., Trouille L., 2010, ApJ, 725, 394
Katz N., Weinberg D. H., Hernquist L., Miralda-Escude J., 1996, ApJ, 457, L57
Kennicutt R. C., Jr, 1998, ARA&A, 36, 189
Kereš D., Vogelsberger M., Sijacki D., Springel V., Hernquist L., 2012, MNRAS, 425, 2027
Kochiashvili I. et al., 2015, A&A, 580, A42
Krogager J.-K., Fynbo J. P. U., Møller P., Ledoux C., Noterdaeme P., Christensen L., Milvang-Jensen B., Sparre M., 2012, MNRAS, 424, L1
Krogager J.-K. et al., 2013, MNRAS, 433, 3091
Krumholz M. R., 2012, ApJ, 759, 9
Kulkarni V. P., Khare P., Som D., Meiring J., York D. G., Péroux C., Lauroesch J. T., 2010, New Astron., 15, 735
Ledoux C., Petitjean P., Fynbo J. P. U., Møller P., Srianand R., 2006, A&A, 457, 71
Lehner N., O'Meara J. M., Fox A. J., Howk J. C., Prochaska J. X., Burns V., Armstrong A. A., 2014, ApJ, 788, 119
Meiring J. D., Lauroesch J. T., Kulkarni V. P., Reroux C., Khare P., York D. G., Crotts A. P. S., 2007, MNRAS, 376, 557
Meiring J. D., Lauroesch J. T., Kulkarni V. P., Peroux C., Khare P., York D. G., 2009, MNRAS, 397, 2037
Modigliani A. et al., 2010, in Silva D. R., Peck A. B., Soifer B. T., eds, Proc. SPIE Conf. Ser. Vol. 7737, Observatory Operations: Strategies, Processes, and Systems III. SPIE, Bellingham, p. 773728
Møller P., 2000, The Messenger, 99, 31
Møller P., Warren S. J., 1998, MNRAS, 299, 661
Møller P., Fynbo J. P. U., Fall S. M., 2004, A&A, 422, L33
Møller P., Fynbo J. P. U., Ledoux C., Nilsson K. K., 2013, MNRAS, 430, 2680
Monier E. M., Turnshek D. A., Rao S., 2009, MNRAS, 397, 943
Morton D. C., 2003, ApJS, 149, 205
Neeleman M., Wolfe A. M., Prochaska J. X., Rafelski M., 2013, ApJ, 769, 54
Nilsson K. K., Møller P., 2009, A&A, 508, L21
Noterdaeme P., Ledoux C., Petitjean P., Srianand R., 2008, A&A, 481, 327
Noterdaeme P., Petitjean P., Ledoux C., Srianand R., 2009, A&A, 505, 1087
Noterdaeme P. et al., 2012, A&A, 540, A63
Noterdaeme P. et al., 2014, A&A, 566, A24
Nussbaumer H., Storey P. J., 1986, A&AS, 64, 545
Palanque-Delabrouille N. et al., 2016, A&A, 589, 2
Pei Y. C., 1992, ApJ, 395, 130
Péroux C., Bouché N., Kulkarni V. P., York D. G., Vladilo G., 2011, MNRAS, 410, 2237
Péroux C., Bouché N., Kulkarni V. P., York D. G., Vladilo G., 2012, MNRAS, 419, 3060
Péroux C., Bouché N., Kulkarni V. P., York D. G., 2013, MNRAS, 436, 2650
Péroux C., Kulkarni V. P., York D. G., 2014, MNRAS, 437, 3144
Peroux C. et al., 2017, MNRAS, 464, 2053
Pontzen A. et al., 2008, MNRAS, 390, 1349
Prochaska J. X., Wolfe A. M., 1997, ApJ, 487, 73
Quiret S. et al., 2016, MNRAS, 458, 4074
Rao S. M., Belfort-Mihalyi M., Turnshek D. A., Monier E. M., Nestor D. B., Quider A. M., 2011, MNRAS, 416, 1215
Sánchez-Ramírez R. et al., 2016, MNRAS, 456, 4488
Schlegel D. J., Finkbeiner D. P., Davis M., 1998, ApJ, 500, 525
Shull J. M., Danforth C. W., Tilton E. M., 2014, ApJ, 796, 49
Vanden Berk D. E. et al., 2001, AJ, 122, 549
Verhamme A., Schaerer D., Atek H., Tapken C., 2008, A&A, 491, 89
Vernet J. et al., 2011, A&A, 536, A105
Warren S. J., Møller P., Fall S. M., Jakobsen P., 2001, MNRAS, 326, 759
Weatherley S. J., Warren S. J., Møller P., Fall S. M., Fynbo J. U., Croom S. M., 2005, MNRAS, 358, 985
Whitaker K. E. et al., 2014, ApJ, 795, 104
Wolfe A. M., Turnshek D. A., Smith H. E., Cohen R. D., 1986, ApJS, 61, 249
Zafar T. et al., 2011, A&A, 532, A51
Zafar T., Péroux C., Popping A., Milliard B., Deharveng J.-M., Frank S., 2013a, A&A, 556, A141
Zafar T., Popping A., Péroux C., 2013b, A&A, 556, A140

This paper has been typeset from a TEX/LATEX file prepared by the author.

Downloaded from https://academic.oup.com/mnras/article/465/2/1613/2525968 by guest on 12 May 2022